Journal of Hepatocellular Carcinoma

Dovepress
Taylor & Francis Group

Open Access Full Text Article

ORIGINAL RESEARCH

# Intravoxel Incoherent Motion Improves the Accuracy of Preoperative Prediction of Vessels Encapsulating Tumor Clusters in Hepatocellular Carcinoma

Min Li[1,2,*], Ge Zhang[2,*], Jing Li[2,*], Yufan Ren[2], Xuan Jin[3], Qiying Ke[4], Congyue Guo[2], Jiaqi Lv[2], Haojun Lu[2], Yongzhou Xu[5], Wen Liang[2], Xianyue Quan[2,6], Xinming Li[2]

[1]Department of Radiology, Chengdu Sixth People's Hospital, Chengdu, Sichuan, People's Republic of China; [2]Department of Radiology, Zhujiang Hospital, Southern Medical University, Guangzhou, People's Republic of China; [3]Department of Radiology, The Fourth Affiliated Hospital, Zhejiang University School of Medicine, Yiwu, Zhejiang, People's Republic of China; [4]Department of Radiology, The First Affiliated Hospital of Guangzhou University of Chinese Medicine, Guangzhou, People's Republic of China; [5]Philips Healthcare, Guangzhou, People's Republic of China; [6]Department of Radiology, Heyou Hospital, Foshan, Guangdong, People's Republic of China

*These authors contributed equally to this work

Correspondence: Xianyue Quan; Xinming Li, Department of Radiology, Zhujiang Hospital, Southern Medical University, Guangzhou, People's Republic of China, Email quanxianyue2014@163.com; lixinmingsmu@163.com



**Purpose:** Hepatocellular carcinoma (HCC) with vessels encapsulating tumor clusters (VETC) pattern presents a higher risk of recurrence and metastasis, and the unique vascular structure of the VETC pattern may affect the perfusion and diffusion, and the effect that can be captured by intravoxel incoherent motion (IVIM). Therefore, this study used preoperative IVIM to predict VETC pattern in HCC and performed preoperative noninvasive recurrence risk stratification.

**Patients and Methods:** Patients with suspicious HCC were included prospectively. Two radiologists independently evaluated radiologic features and measured apparent diffusion coefficient (ADC), true diffusion coefficient (*D*), pseudo-diffusion coefficient (*D**), and pseudo-diffusion fraction (*f*). Logistic regression analyses were used to identify the predictors associated with the VETC pattern. Receiver operating characteristic (ROC) curve analyses were conducted to assess the predictive performance. Recurrence-free survival was evaluated using the Kaplan–Meier analysis and the Log rank test.

**Results:** The consecutive cohort included 116 patients (mean age, 55 years ± 11, 94 men). Twenty-nine of the 116 HCC (25.0%) were VETC HCC. The *f* value (odds ratio [OR], 0.791; $p < 0.001$), serum α-fetoprotein level (>400 ng/mL) (OR, 2.962; $p = 0.042$), and intratumor necrosis (OR, 6.022; $p = 0.015$) were independent predictors of the VETC pattern. These characteristics were used to construct the combined model with area under the ROC curve of 0.854. Additionally, adding the *f* value to the conventional imaging-clinical model substantially improved its predictive performance ($p < 0.001$). Moreover, patients with the combined model classified as VETC HCC also had a higher risk of early recurrence than those with non-VETC HCC ($p < 0.001$).

**Conclusion:** IVIM enhances the accuracy of preoperative prediction of the VETC pattern and provides preoperative noninvasive risk stratification for HCC recurrence.

**Keywords:** hepatocellular carcinoma, diffusion-weighted imaging, recurrence-free survival, vessels encapsulating tumor clusters, intravoxel incoherent motion

## Introduction

Hepatocellular carcinoma (HCC) accounts for the majority of primary malignant liver cancers and is the third leading cause of cancer-related deaths worldwide.[1,2] Hepatectomy, ablation, and liver transplantation are effective treatments for early-stage HCC.[3–5] However, the recurrence rate within 5 years of hepatectomy is approximately 40–70%.[6,7] The high rate of recurrence and metastasis significantly impacts the prognosis of patients with HCC.[8] HCC with vessels encapsulating tumor clusters



Received: 16 February 2025
Accepted: 25 May 2025
Published: 11 June 2025

(VETC) pattern, characterized by sinusoid-like vessels that isolate and encapsulate individual tumor clusters, forming a cobweb-like pattern,[9] presents a higher risk of recurrence and metastasis.[8,10] Several case–control studies have demonstrated that VETC HCC exhibit a more favorable therapeutic response to sorafenib, resection after recurrence, and adjuvant transcatheter arterial chemoembolization, effectively improving its prognosis.[9,11–13] Therefore, the accurate identification of VETC is crucial for developing individualized treatment for HCC. However, accurate identification of VETC can currently only be assessed via resection or transplantation specimens, not by tissue microarray or liver biopsy.[9] Noninvasive radiologic identification of VETC patterns is currently under investigation.

Currently, radiologic prediction methods for VETC HCC are mainly based on conventional radiologic features, radiomics features, or texture analyses. Previous studies have demonstrated that tumors larger than 5 cm, intratumor necrosis, non-rim diffuse and heterogeneous arterial-phase hyperenhancement (APHE), a tumor-to-liver signal intensity ratio 1.135 or greater on arterial phase images, and a tumor-to-liver signal intensity ratio 0.585 or less on hepatobiliary phase (HBP) images are associated with VETC pattern.[14–18] The unique vascular structure of the VETC pattern may affect tumor perfusion and diffusion microenvironment. Intravoxel incoherent motion (IVIM) evaluates true molecular diffusion and microcirculation of blood using a biexponential model,[19] providing a more detailed assessment of tumor microenvironment than that by conventional diffusion-weighted imaging (DWI), which uses a monoexponential model. IVIM distinguishes true diffusion from perfusion effects, thereby enhancing the sensitivity for detecting vascular patterns and tissue cellularity.[19] However, the effectiveness of IVIM in predicting VETC patterns in HCC has yet to be established.

Thus, this study aimed to assess the value of preoperative IVIM in predicting VETC HCC and investigate its predictive value for HCC recurrence in patients who had undergone surgical resection.

# Materials and Methods

## Patients

This prospective study was approved by the appropriate institutional review board, and written informed consent was obtained from all patients. Between April 2018 and August 2022, we prospectively recruited 161 participants suspected of having HCC, identified via ultrasonography or computed tomography (CT), who underwent preoperative gadolinium ethoxybenzyl diethylenetriamine pentaacetic acid (Gd-EOB-DTPA)-enhanced magnetic resonance imaging (MRI) and IVIM sequence examination. The inclusion criteria were as follows: (a) no prior treatment for liver lesions (for patients with early-stage HCC who had undergone other treatments, there was no evidence to determine whether those treatments would affect the recognition of VETC patterns); (b) no contraindication to MRI examinations; and (c) age ≥ 18 years. Of the 161 participants recruited, 45 were excluded for the following reasons: (a) hepatectomy not possible due to the late stage of the tumor (n = 24). Our study was based on accurate assessment of the VETC pattern, which currently requires resection or transplantation specimens; thus, we excluded late-stage patients who were no longer eligible for surgery; (b) tumor size < 10 mm (n = 5), for which the region of interest (ROI) could not be precisely obtained; (c) poor radiologic or pathologic images for evaluation (n = 4); (d) Gd-EOB-DTPA-enhanced MRI and IVIM scan performed more than 2 weeks prior to the surgery (n = 3); and (e) hepatic lesions pathologically diagnosed as non-HCC (n = 9)(Figure 1).

Clinical and laboratory data, including age; sex; cause of underlying liver diseases; and preoperative serum α-fetoprotein (AFP), total bilirubin, alanine aminotransferase (ALT), aspartate aminotransferase (AST), and γ-glutamyltransferase (γ-GT) levels, were collected.

## MRI Examination

Liver MRI was performed using a 3.0-T MRI scanner (Ingenia, Philips Healthcare, Best, Netherlands) equipped with a dedicated 32-channel system. The patients were instructed to withhold oral ingestion of food and fluids for 4 h before the examination. The MRI protocol included a fat-suppressed turbo spin-echo T2-weighted sequence, mDIXON T1-weighted sequences, IVIM and enhanced scanning. IVIM registration was performed using a single-shot echo-planar imaging sequence with respiratory gating before contrast injection. The 9 *b* values ranged from 0 to 1000 s/mm$^2$ (0, 25, 50, 75, 100, 150, 300, 700, and 1000) with corresponding *b*-factor averages of 1, 1, 1, 1, 1, 1, 1, 3 and 4. Enhanced scanning using Gd-EOB-DTPA (Primovist, Bayer Schering Pharma, AG, Berlin, Germany) was performed, and images

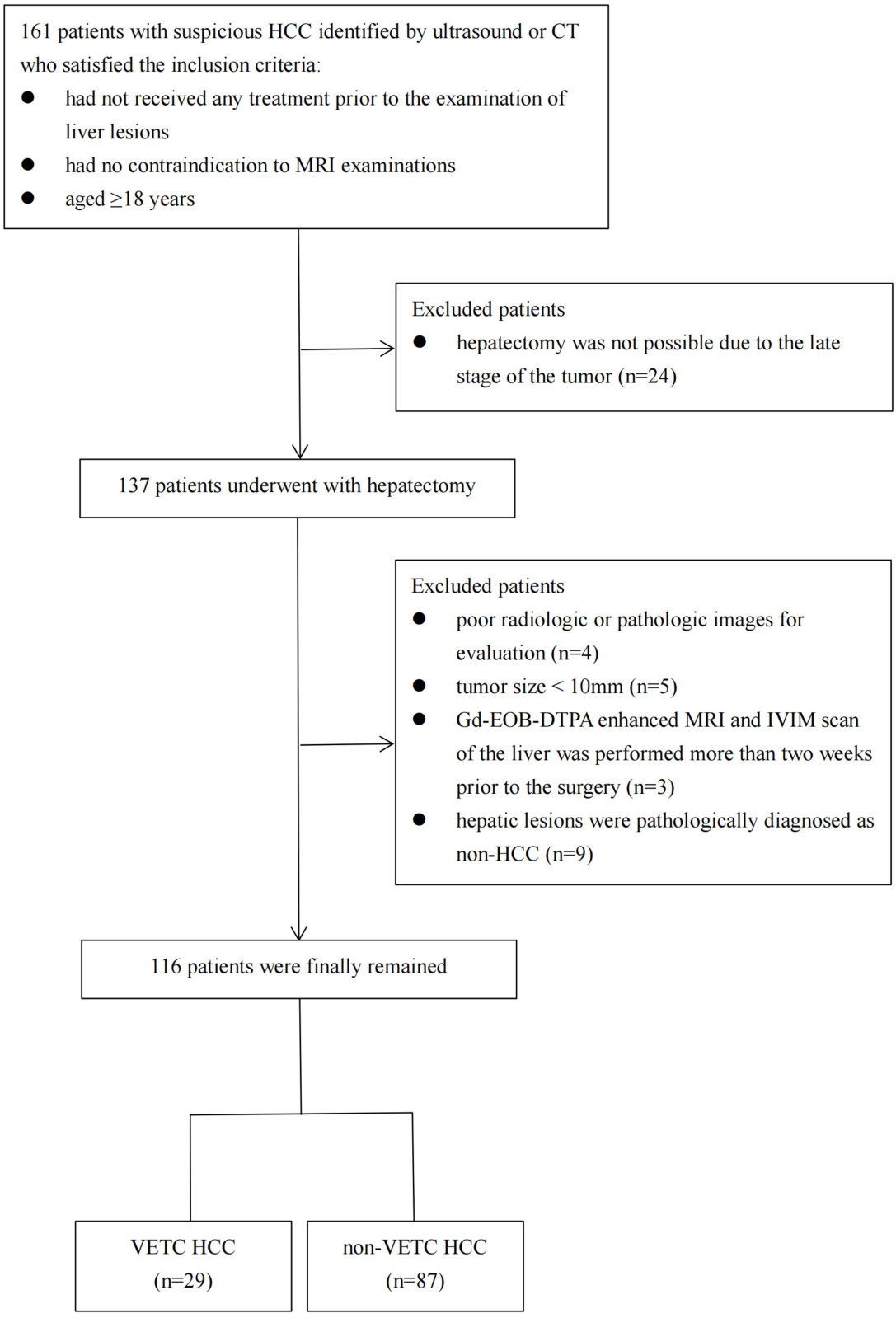


**Figure 1** Flowchart of the study.


https://doi.org/10.2147/JHC.S519223

of the arterial, portal venous, transitional, and hepatobiliary phases were obtained 20s, 1 min, 3 min, and 20 min, respectively, after contrast injection of 0.1 mmol/kg at a rate of 2 mL/s. MRI parameters are presented in Table 1.

## Radiologic Feature Analysis

All MRI images were independently assessed by two radiologists with 8 and 15 years of experience in hepatic imaging. The radiologists were blinded to the histopathologic findings and laboratory information of the patients. In cases of disagreement between the radiologists, a joint review was performed until a consensus was reached. The following radiologic characteristics of each HCC lesion were evaluated referring to previous studies,[15,20–22] the liver imaging reporting and data system (LI-RADS) v. 2018,[23] and LI-RADS lexicon (terms and definitions):[24] (a) tumor size, defined as the largest cross-sectional diameter of the lesion; when more than one lesion was present, the largest lesion was selected for measurement; (b) fat in mass, defined as signal loss on opposed-phase image compared with in-phase image; (c) non-rim APHE, defined as presence of enhancement significantly greater than that of the background liver during the arterial phase, where the enhancement was not confined to the periphery of the tumor; (d) intratumor arteries, defined as enhanced blood vessels visible within tumor during the arterial phase; (e) capsule, defined as a thin low-signal ring surrounding the tumor on the arterial phase and a high-signal structure with linear enhancement on portal or delayed phase images; (f) intratumor necrosis, defined as a central high-signal area on fat-suppressed T2-weighted images and a low-signal area on T1-weighted images, with no enhancement on postcontrast T1-weighted images, involving more than 20% of the tumor area at the level of the largest cross-sectional diameter; (g) intratumor hemorrhage, defined as a high-signal area on T1-weighted images without signal loss on opposed-phase or fat-suppressed images; (h) irregular tumor margin, defined as tumor with irregular margin that had budding portions at the periphery; (i) non-peripheral washout, defined as non-peripheral visual reduction in enhancement from the earlier to the later phase, resulting in hypoenhancement relative to the liver; (j) peritumor low signal on HBP; and (k) satellite nodules, defined as tumor less than 2 cm in diameter and no more than 2 cm from the maximum tumor.

## IVIM and DWI MRI Analysis

The Medical Imaging Interaction Toolkit (MITK, Nolden et al, v. 2018) postprocessing software was used to calculate the IVIM parameter maps using the following equation: $S_b/S_0 = (1-f)\exp(-bD) + f\exp[-b(D+D^*)]$. In this study, the ROI outlined for each patient included the entire tumor. The two diagnostic radiologists outlined the tumor margin layer-by-layer based on the original IVIM images ($b$ = 0 s/mm$^2$) to be used as ROIs, ensuring to avoid areas of tumor necrosis, hemorrhage, and vascular structures as much as possible. The $D$, $f$, and $D$* values were automatically calculated using the software. The apparent diffusion coefficient (ADC) value was calculated based on $b$ = 0 s/mm$^2$ and $b$ = 700 s/mm$^2$ of IVIM. The ROI for the ADC was outlined using the MITK software in the same manner as that described above. The average value of each parameter across all tumor sections was used for further statistical analyses. The method for obtaining the ROIs is shown in Figure S1.

**Table 1** MRI Parameters of IVIM, TIWI, T2WI and Enhanced Image

| Parameters | Axial IVIM | Axial T1WI | Axial T2WI | Axial Enhanced Image |
|---|---|---|---|---|
| Repetition time (ms) | 2691 | 3.2 | 561 | 3.2 |
| Echo time (ms) | 51 | 1.12 and 2.0 | 70 | 1.12 and 2.0 |
| Field of view (mm$^2$) | 300 × 381 | 320 × 280 | 320 × 376 | 280 × 292 |
| Flip angle (°) | 90 | 10 | 90 | 10 |
| Matrix (frequency × phase) | 120 × 146 | 180 × 158 | 180 × 164 | 156 × 163 |
| Slice thickness (mm) | 6 | 4 | 6 | 5 |
| Slice gap (mm) | 0.6 | −2 | 1 | −2.5 |
| Number of slices | 18 | 100 | 28 | 64 |
| *b* values | 0, 25,50,75,100,150,300,700,1000 | | | |

**Abbreviations**: IVIM, intravoxel incoherent motion; MRI, magnetic resonance imaging; T1WI, T1-weighted image; T2WI, T2-weighted image.

## Histopathologic Examination

The examined histopathologic features included the Edmonson–Steiner grade, satellite nodules, and microvascular invasion (MVI). The VETC pattern was defined as the presence of sinusoid-like vessels that encapsulate individual tumor clusters and form cobweb-like pattern in any tumor region, as observed through CD34 immunostaining.[9]

## Follow-up After Surgical Resection

Patients underwent routine follow-ups every 3–6 months postoperatively. Radiologic follow-up included enhanced CT or MRI, and any suspicious hepatic lesions were evaluated using at least two imaging modalities (contrast-enhanced CT or MRI, ultrasonography, or hepatic angiography). The follow-up endpoint time was defined as the first occurrence of the following conditions: (1) new intrahepatic lesions detected on imaging and consistent with the presentation of HCC; (2) extrahepatic metastases detected; and/or (3) pathological findings of the lesion confirming HCC.

## Statistical Analysis

Continuous variables were summarized using means and standard deviations and compared using Student's *t* test. Categorical variables were presented using counts and percentages and compared using the $\chi^2$ test or Fisher's exact test. The agreement between the observers for each MRI feature was assessed using the intraclass correlation coefficient (ICC) and Kappa. Logistic regression analyses and model selection were performed using stepwise criteria to identify independent predictors of the VETC pattern. Odds ratio (OR) and 95% confidence interval (CI) were calculated. Receiver operating characteristic (ROC) curve analyses were conducted to evaluate the predictive performance, and model performance was compared using the DeLong test. The area under the ROC curve (AUC), sensitivity and specificity were determined using the Youden index. Recurrence-free survival (RFS) was evaluated and compared using the Kaplan–Meier method and Log rank test. SPSS software (v. 25.0; IBM, Armonk, NY, USA) and R software (v. 3.4.1; The R Foundation for Statistical Computing, Vienna, Austria) were used for all statistical analyses. A statistically significant difference was defined as a p value less than.05.

# Results

## Clinical and Pathologic Characteristics

During the study period, 116 consecutive patients were included: 94 (81.0%) men (mean age, 54 ± 10 years; range, 35–80 years) and 22 (19.0%) women (mean age, 57 ± 14 years; range, 30–74 years). Among the 116 patients, 29 (25.0%) had VETC HCC. Regarding the clinical and pathological characteristics, statistical significance was exclusively observed in elevated preoperative AFP levels between VETC HCC (13/29) and non-VETC HCC (18/87) (p = 0.011) (Table 2).

## Radiologic Features and Diffusion Parameters

Among routine MRI features, intratumor necrosis (p = 0.003) and intratumor arteries (p = 0.001) showed statistically significant differences between the VETC HCC and non-VETC HCC groups. Among the IVIM and DWI parameters, the ADC and *f* values were remarkably lower in the VETC HCC group (Figure 2) than in the non-VETC HCC group

**Table 2** Comparison of Clinical and Pathological Characteristics of VETC and Non-VETC HCC

| Characteristics | VETC HCC(n=29) | Non-VETC HCC(n=87) | p value |
|---|---|---|---|
| Clinical characteristics | | | |
| Age(years)[a] | 52.14 ± 11.33 | 55.57 ± 10.49 | 0.137 |
| Sex(men) | 23(79.3) | 71(81.6) | 0.784 |
| Etiology | | | 0.421 |
| Hepatitis B virus | 25(86.2) | 69(79.3) | |
| Other | 4(13.8) | 18(20.7) | |

(*Continued*)

**Table 2** (Continued).

| Characteristics | VETC HCC(n=29) | Non-VETC HCC(n=87) | p value |
|---|---|---|---|
| Preoperative laboratory results | | | |
| Total bilirubin, > 21(μmol/L)[b] | 8(27.6) | 10(11.5) | 0.076 |
| AFP, > 400(ng/mL) | 13(44.8) | 18(20.7) | 0.011 |
| ALT, > 50(IU/L) | 6(20.7) | 14(16.1) | 0.570 |
| AST, > 40(IU/L) | 12(41.4) | 23(26.4) | 0.129 |
| γ-GT, > 60(IU/L) | 15(51.7) | 32(36.8) | 0.156 |
| Pathological characteristics | | | |
| Edmondson-Steiner grade | | | 0.896 |
| G1-G2 | 23(79.3) | 68(78.2) | |
| G3-G4 | 6(20.7) | 19(21.8) | |
| MVI | | | 0.377 |
| Negative | 9(31.0) | 35(40.2) | |
| Positive | 20(69.0) | 52(59.8) | |

**Notes**: [a]Data are means ± standard deviation. Unless otherwise specified, data in parentheses are percentages. [b]Data were compared using Fisher's exact test. The age was compared using the independent-samples *t* test. Except where indicated, data were compared using the $\chi^2$ test.

**Abbreviations**: AFP, α-fetoprotein; ALT, alanine aminotransferase; AST, aspartate aminotransferase; γ-GT, γ-glutamyltransferase; HCC, hepatocellular carcinoma; MVI, microvascular invasion; VETC, vessels encapsulating tumor cluster.

(Figure 3) ($p < 0.001$). However, $D^*$ ($p = 0.406$) and $D$ ($p = 0.084$) values were not statistically significantly different between the two groups. For all radiologic features and diffusion parameters, the interobserver agreements were good or excellent (Tables 3 and S1).

## Predictors for VETC Pattern

In the univariable analysis, several factors showed statistical significance between the VETC HCC and non-VETC HCC groups: serum AFP level higher than 400 ng/mL (OR, 3.115; 95% CI: 1.270–7.638; p = 0.013), intratumor arteries (OR, 4.480;

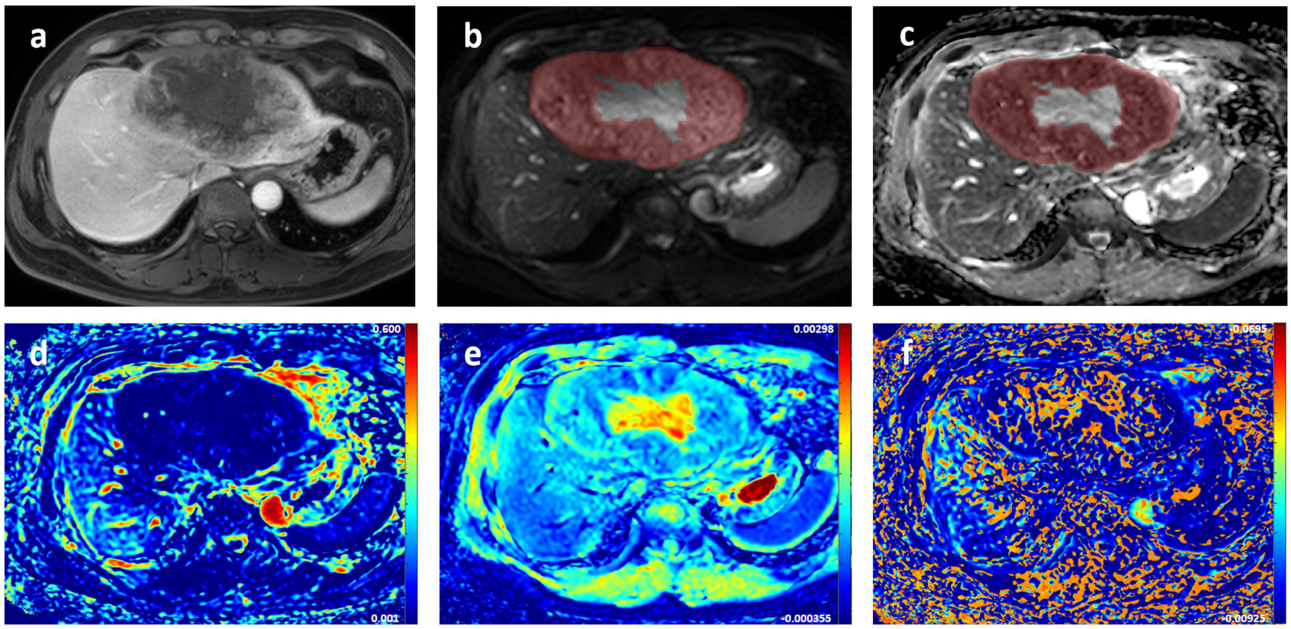


**Figure 2** A 44-year-old male patient with VETC HCC. (**a**) Portal venous phase. (**b**) ROI schematic at $b = 0$ s/mm$^2$ for IVIM. (**c**) ADC map; ADC value for the lesion was $0.82\times10^{-3}$ mm$^2$/s. (**d**) *f* map: *f* value for the lesion was 8.35%. (**e**) *D* map; *D* value for the lesion was $0.81\times10^{-3}$ mm$^2$/s. (**f**) $D^*$ map; $D^*$ value for the lesion was $42.60\times10^{-3}$ mm$^2$/s.

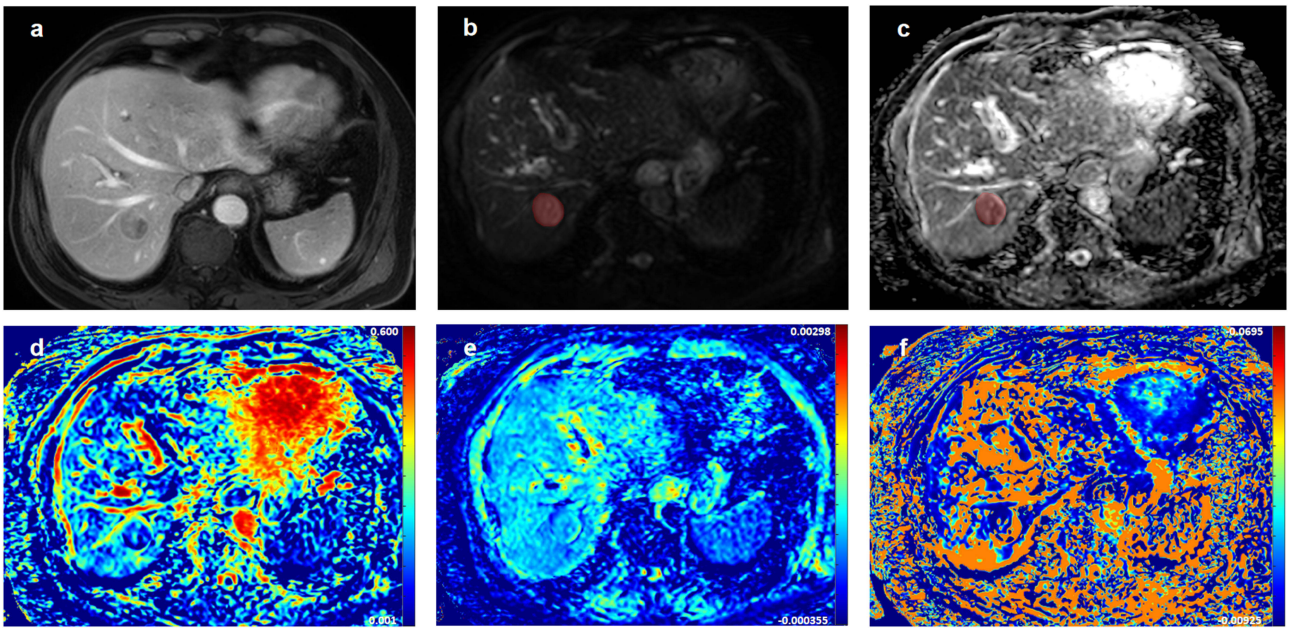


**Figure 3** A 69-year-old male patient with non-VETC HCC. (**a**) Portal venous phase. (**b**) ROI schematic at $b$ = 0 s/mm$^2$ for IVIM. (**c**) ADC map; ADC value for the lesion was 1.07×10$^{-3}$ mm$^2$/s. (**d**) $f$ map; $f$ value for the lesion was 17.19%. (**e**) $D$ map; $D$ value for the lesion was 1.01×10$^{-3}$ mm$^2$/s. (**f**) $D$* map, $D$* value for the lesion was 46.56×10$^{-3}$ mm$^2$/s.

95% CI: 1.792–11.202; p = 0.001), intratumor necrosis (OR, 5.833; 95% CI: 1.639–20.763; p = 0.006), $f$ value (OR, 0.801; 95% CI: 0.712–0.900; p < 0.001), and ADC value (OR, 0.022; 95% CI: 0.001–0.380; p = 0.009). The multivariable logistic regression analysis revealed that intratumor necrosis (OR, 6.022; 95% CI: 1.427–25.413; p = 0.015), serum AFP levels higher

**Table 3** MRI Findings and Their Relationship with VETC HCC

| MRI Findings | ICC/Kappa | VETC HCC (n=29) | non-VETC HCC (n=87) | p value |
|---|---|---|---|---|
| Radiologic features | | | | |
| Tumor size[a] | 0.989 | 68.59 ± 40.84 | 51.90 ± 31.58 | 0.051 |
| Fat in mass | 0.802 | 5(17.2) | 21(24.1) | 0.441 |
| Non-rim APHE | 0.760 | 26(89.7) | 68(78.2) | 0.274 |
| Intratumor arteries | 0.859 | 14(48.3) | 15(17.2) | 0.001 |
| Capsule | 0.856 | 19(65.5) | 51(58.6) | 0.511 |
| Intratumor necrosis | 0.860 | 26(89.7) | 52(59.8) | 0.003 |
| Intratumor hemorrhage | 0.851 | 12(41.4) | 30(34.5) | 0.503 |
| Irregular tumor margin | 0.827 | 22(75.9) | 63(72.4) | 0.716 |
| Non-peripheral washout | 0.811 | 24(82.8) | 67(77.0) | 0.696 |
| Peritumor low signal on HBP | 0.903 | 11(37.9) | 28(32.2) | 0.570 |
| Satellite nodules | 0.879 | 7(24.1) | 14(16.1) | 0.330 |
| IVIM and DWI parameters | | | | |
| $f$[a] | 0.844 | 13.07 ± 4.55 | 19.66 ± 7.95 | <0.001 |
| $D$[a] | 0.817 | 0.92 ± 0.21 | 0.98 ± 0.15 | 0.084 |
| $D$*[a] | 0.821 | 50.85 ± 37.41 | 44.18 ± 37.13 | 0.406 |
| ADC[a] | 0.873 | 1.09 ± 0.11 | 1.20 ± 0.20 | <0.001 |

**Notes**: [a]Data are means ± standard deviation. Unless otherwise specified, data in parentheses are percentages. The tumor size, $f$, $D$, $D$*, and ADC were compared using the independent-samples $t$ test. Except where indicated, data were compared using the $\chi^2$ test. The tumor size is in the unit of mm; ADC, $D$, and $D$* are in units of 10$^{-3}$ mm$^2$ /s; and $f$ is in the unit of 100%.

**Abbreviations**: ADC, apparent diffusion coefficient; $D$, true diffusion coefficient; $D$*, pseudo-diffusion coefficient; DWI, diffusion-weighted imaging; $f$, pseudo-diffusion component fraction; HBP, hepatobiliary phase; HCC, hepatocellular carcinoma; ICC, interclass correlation coefficient; IVIM, intravoxel incoherent motion; APHE, arterial-phase hyperenhancement; VETC, vessels encapsulating tumor clusters.


https://doi.org/10.2147/JHC.S519223

than 400 ng/mL (OR, 2.962; 95% CI: 1.038–8.448; p = 0.042), and *f* value (OR, 0.791; 95% CI: 0.697–0.896; p < 0.001) were independently associated with VETC HCC (Table 4). A visual nomogram illustrating these predictors is shown in Figure 4. When the model was constructed using only *f* value, the AUC value was 0.782 (95% CI: 0.686–0.877). When combining intratumor necrosis and higher serum AFP levels into a conventional imaging-clinical model, the ROC curve analysis yielded an AUC of 0.707 (95% CI: 0.606–0.808). Adding the *f* value to create a combined model increased the AUC to 0.854 (95% CI: 0.772–0.935), with a sensitivity of 86.2% and specificity of 73.6%. The DeLong test indicated that the combined model achieved superior predictive performance compared with that of the conventional imaging-clinical model (p < 0.001) (Figure 5). Additional data for comparison of the two groups are presented in Table S2. And the Youden index was used to establish a cutoff value of 15.7% for the *f* value.

### Prognosis

The 116 patients who were followed up had a median RFS of 24 months (range, 1–64 months), with a total of 36 recurrences. In the VETC HCC group, recurrence occurred in 16 patients (55.2%), with 15 (94.0%) experiencing early recurrence (within 2 years). In contrast, in the non-VETC HCC group, recurrence occurred in 20 patients (23.0%), with 17 (85.0%) experiencing early recurrence. The Log rank test indicated that patients classified with the VETC HCC pathology had a significantly higher risk of recurrence than that in those with non-VETC HCC (p < 0.001) (Figure 6a). Furthermore, patients classified as having VETC HCC according to the combined model also showed a higher risk of recurrence than that in those classified as having non-VETC HCC (p < 0.001) (Figure 6b).

## Discussion

HCC presenting with a VETC pattern is known for its aggressive nature and higher recurrence rates. Diagnosis of VETC still relies on pathologic immunohistochemistry, as the small amount of pathologic tissue obtained through liver biopsy cannot accurately determine the status of VETC in HCC.[9] Therefore, noninvasive and accurate preoperative prediction of VETC is crucial for personalized clinical management. In our study, 25.0% of HCC cases were VETC-positive,

**Table 4** Univariable and Multivariable Analyses of the Risk Factors of VETC

| Risk Factors | Univariable Analysis | | | Multivariable Analysis | | |
|---|---|---|---|---|---|---|
| | OR | 95% CI | p value | OR | 95% CI | p value |
| Age(years) | 0.970 | 0.932–1.010 | 0.138 | | | |
| Hepatitis B infection | 1.630 | 0.503–5.285 | 0.415 | | | |
| AFP, > 400(ng/mL) | 3.115 | 1.270–7.638 | 0.013 | 2.962 | 1.038–8.448 | 0.042 |
| ALT, > 50(IU/L) | 1.360 | 0.469–3.946 | 0.571 | | | |
| AST, > 40(IU/L) | 1.964 | 0.815–4.732 | 0.132 | | | |
| Tumor size | 1.013 | 1.001–1.025 | 0.051 | | | |
| Intratumor steatosis | 0.665 | 0.222–1.931 | 0.443 | | | |
| Rim-APHE | 1.659 | 0.595–4.624 | 0.333 | | | |
| Intratumor arteries | 4.480 | 1.792–11.202 | 0.001 | | | |
| Capsule | 1.341 | 0.558–3.222 | 0.512 | | | |
| Intratumor necrosis | 5.833 | 1.639–20.763 | 0.006 | 6.022 | 1.427–25.413 | 0.015 |
| Intratumor hemorrhage | 1.341 | 0.567–3.173 | 0.504 | | | |
| Peritumor low signal on HBP | 1.288 | 0.537–3.088 | 0.571 | | | |
| Satellite nodules | 1.659 | 0.595–4.624 | 0.333 | | | |
| *f* | 0.801 | 0.712–0.900 | <0.001 | 0.791 | 0.697–0.896 | <0.001 |
| *D* | 0.105 | 0.007–1.525 | 0.099 | | | |
| *D** | 1.004 | 0.994–1.015 | 0.419 | | | |
| ADC | 0.022 | 0.001–0.380 | 0.009 | | | |

**Abbreviations**: ADC, apparent diffusion coefficient; AFP, α-fetoprotein; ALT, alanine aminotransferase; AST, aspartate aminotransferase; CI, confidence interval; *D*, true diffusion coefficient; *D**, pseudo-diffusion coefficient; *f*, pseudo-diffusion component fraction; HBP, hepatobiliary phase; OR, odds ratio; APHE, arterial-phase hyperenhancement; VETC, vessels encapsulating tumor clusters.

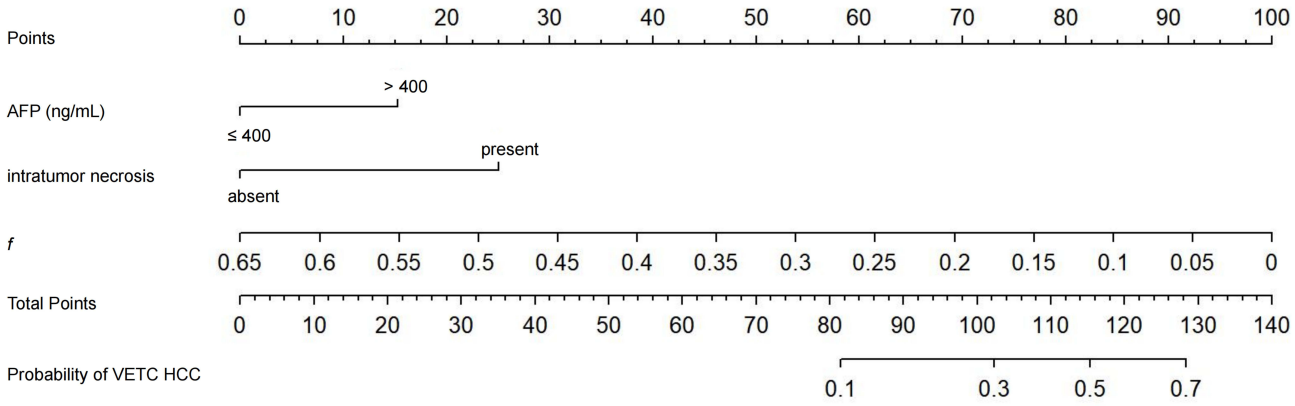


**Figure 4** Nomogram representing the visual outcome of VETC HCC.

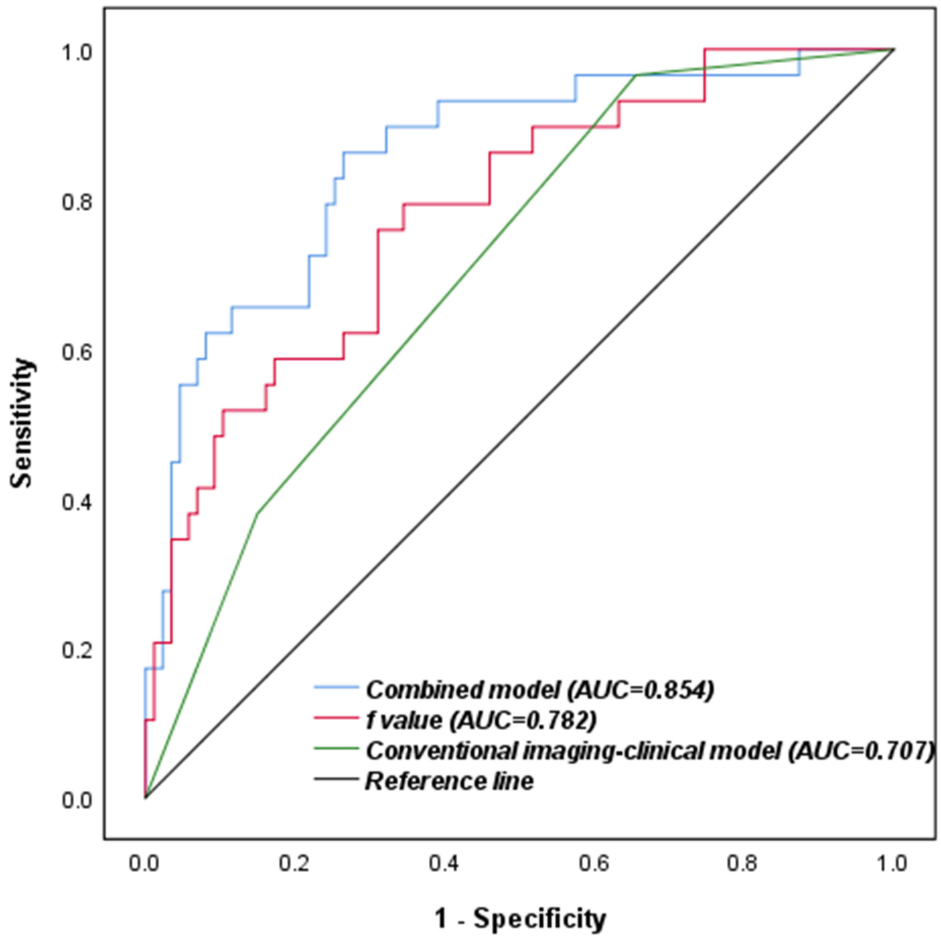


**Figure 5** Comparison of the ROC curve analysis between the combined model, the conventional imaging-clinical model and *f* value.

consistent with previously reported rates ranging from 14.2% to 56.3% in cohorts undergoing curative-intent resection.[9] Multivariable analysis identified several risk factors associated with VETC HCC in our cohort, including *f* value from the IVIM model, preoperative AFP level higher than 400 ng/mL, and intratumor necrosis. Furthermore, patients classified as having VETC HCC based on our combined model exhibited a significant higher risk of recurrence compared to that in

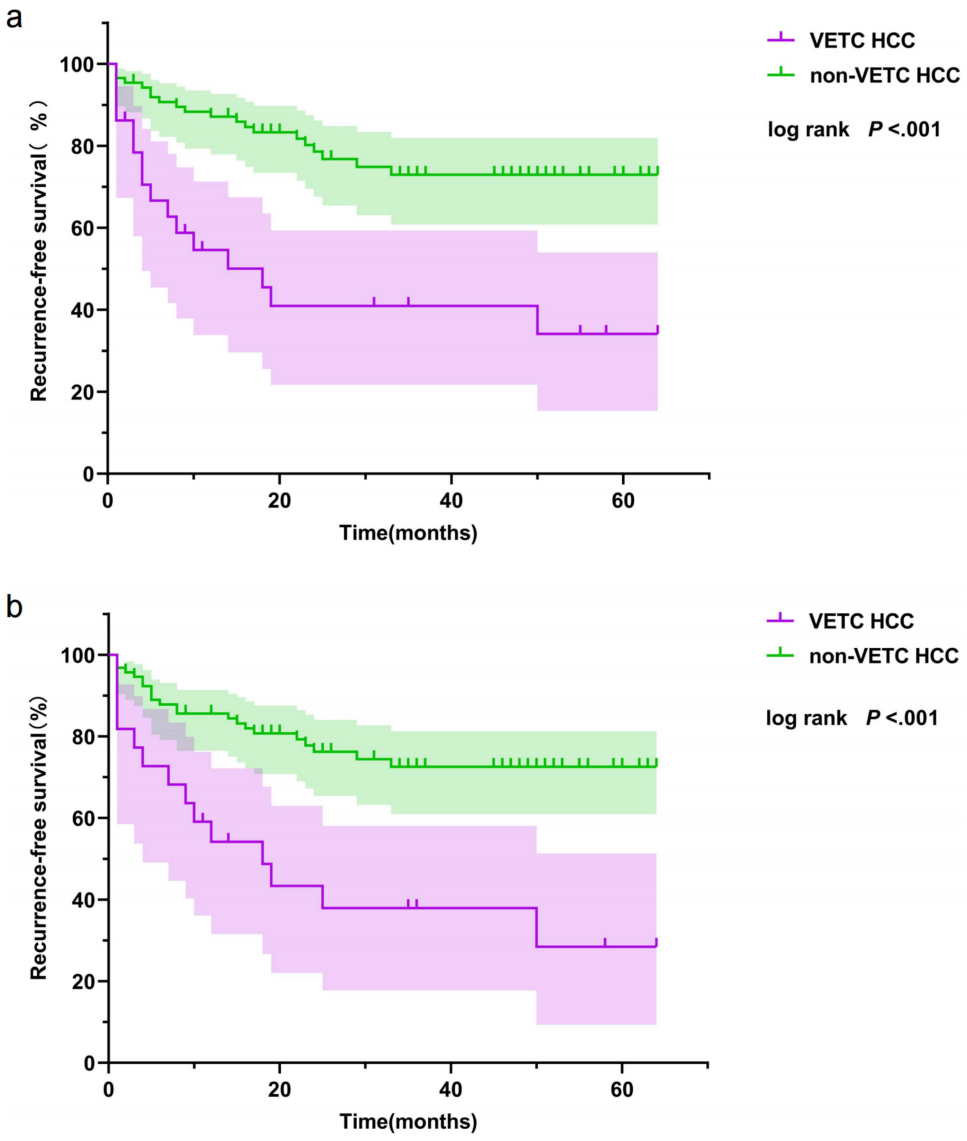


**Figure 6** Kaplan–Meier curves for RFS based on pathological and model grouping. (**a**) Comparison of RFS between VETC HCC and non-VETC HCC grouped by pathological diagnosis. (**b**) Comparison of RFS between VETC HCC and non-VETC HCC grouped by the combined model diagnosis.

those classified as having non-VETC HCC. This underscores the utility of the combined model in the noninvasive prediction of risk stratification for postoperative recurrence in HCC. The *f* value derided from IVIM is often lower in VETC HCC, reflecting its unique vascular structure and hypoperfusion characteristics. This study demonstrated the utility of a combined model based on IVIM in predicting VETC HCC and assessing risk stratification for postoperative recurrence, highlighting its role in assessing the tumor microenvironment.

In the IVIM technique, lower *b* values were mainly used to assess perfusion, while higher *b* values provided more effective diffusion information, facilitating the separation of these two effects.[19] Therefore, 9 *b* values (0, 25, 50, 75, 100, 150, 300, 700, and 1000) were chosen for IVIM parameter estimation in this study. These *b* values were chosen to balance the perfusion effect, represented by lower *b* values, and the diffusion effect, represented by higher *b* values, enabling effective differentiation between microvascular perfusion and tumor diffusion in HCC. Considering that an excessive number of *b* values may lead to longer scanning times and potential signal-to-noise ratio issues, the selected range ensured a balance between parameter fitting accuracy and clinical feasibility. IVIM separated diffusion and perfusion signals through multi *b* value acquisition and biexponential model fitting, achieving a more accurate portrayal

of the tissue microenvironment, and at the same time, three parameters can be obtained, and the combination of multiple parameters can improve the diagnostic specificity, which were the advantages compared with DWI. At the same time, IVIM can also be used to assess diffusion and perfusion microenvironment non-invasively compared with conventional perfusion imaging, avoiding the use of contrast material, and providing a means of examination for patients with renal insufficiency, contrast allergy, and the need for multiple follow-up of tumor treatment.

In this study, we found that intratumor necrosis was independently associated with VETC patterns, consistent with previous findings.[14] HCC with a VETC pattern is characterized by rapid growth, tumor expansion, increased diffusion distance from supplying vessels, and higher cell density due to rapid proliferation, leading to a hypoxic tumor microenvironment.[10] This rapid decrease in perfusion towards the center of the tumor leads to central necrosis. Our study demonstrated that, compared to non-VETC HCC, VETC HCC had a lower *f* value from IVIM, indicating tumor hypoperfusion characteristic of VETC HCC. This hypoperfusion results in an increased incidence of intratumor necrosis within VETC HCC lesions.

Previous studies have indicated that neovascularization in tumors is mainly concentrated at the periphery of the tumor.[25] Consistent with pathologic considerations, the ROI in the current study was focused on tumor parenchyma, excluding the tumor necrotic area. This region has vigorous tumor growth, higher cell density, and increased oxygen demand, influencing the perfusion microenvironment of VETC HCC.[10,25] VETC HCC primarily metastasizes through tumor clusters surrounded by endothelial cells,[8] which can occlude small blood vessels and affect tumor perfusion. Studies have shown that poorer histologic differentiation results in a lower *f* value[26,27] and that VETC HCC has a higher proportion of poorly differentiated HCC,[14] which may be attributable to the lower *f* value of VETC HCC. Tumors with VETC patterns exhibit increased expression of carbonic anhydrase IX (a marker of hypoxia),[9] confirming that VETC HCC undergoes hypoperfusion. However, Huang et al[10] obtained contrasting results, demonstrating that the VETC pattern was substantially associated with a higher density of intratumor microvasculature and that the *f* value was positively correlated with angiogenesis.[28] This discrepancy might be related to several factors. First, the tumor microenvironment is complex and dynamic, and VETC occurs early in tumor development and does not increase exponentially with tumor growth. Second, only a portion of the tumor was selected as the subject. However, HCC is typically a hypervascular and heterogeneous lesion,[10,29] which may not fully reflect the overall perfusion of VETC HCC.

In the multivariable analysis, only the *f* value derived from IVIM independently predicted VETC HCC, whereas the *D* value from IVIM quantifying diffusion showed no statistical difference. The VETC pattern represents a pathologic classification of HCC closely associated with vascular characteristics that might affect tissue perfusion. ADC value primarily reflected the effects of tissue diffusion, in the present study it was found that ADC value showed a difference in univariate analysis, but it did not emerge as an independent risk factor for VETC in our multivariable analysis. We suspect that the effect of the VETC pattern on diffusion was not remarkable so the contribution of ADC value to predicting VETC patterns is weakened by the *f* value. Moreover, according to Le Bihan et al,[30] the blood flow in the capillaries mimicked a diffusion process, which may have implications for diffusion measurements. The ADC value is highly influenced by perfusion and may not be a true reflection of tissue diffusion.

This study revealed that intratumor necrosis, lower *f* values, and higher AFP levels are associated with a higher risk of recurrence following HCC curative resection. Previous studies have demonstrated that a lower *f* value is associated with poor differentiation and that HCC with MVI tends to have a lower *f* value.[26,27] The present study revealed that a low *f* value is an independent predictor of VETC HCC, which is also associated with a poor prognosis of patients with HCC.[8,10,31–36] Zhang et al[27] demonstrated that HCC with *f* values ≤23.4% had higher recurrence rates. However, the present study suggested an optimal cutoff of the *f* value to be ≤ 15.7%. This difference might be related to the varying influence of different pathological types on tumor perfusion in HCC and the proportions of these types in the study population. Rhee et al[37] reported that, compared with non-APHE HCC, tumor necrosis in HCC was associated with rim-APHE, which demonstrated aggressive histopathologic features and led to a worse prognosis,[38,39] including a higher frequency of MVI, higher proportions of VETC, and a macrotrabecular-massive pattern. Another study indicated that rim-APHE may help identify proliferative HCC.[20] Moreover, a high preoperative AFP level (> 400 ng/mL) was associated with HCC recurrence, consistent with previous findings.[27,40,41]

This study has some limitations. First, the findings were derived from patients who underwent curative resection and were not representative of the entire population of patients with HCC; therefore, the value of the model in non-surgically treated patients deserves further exploration. Second, the total number of patients included in this study was relatively small; therefore, future research should focus on expanding the sample size. Third, all data were collected from a single center, and the model used to estimate survival was applied to the same group on which it was trained; therefore, validation of the results in other centers is needed.

## Conclusion

Our results suggest that IVIM improves the accuracy of preoperative prediction of the VETC pattern, offering useful prognostic information. This improvement in early diagnosis could inform more tailored treatment plans, thereby optimizing patient outcomes. Therefore, IVIM emerges as a pivotal tool in the clinical management of VETC HCC.

## Abbreviations

ADC, apparent diffusion coefficient; AFP, α-fetoprotein; ALT, alanine aminotransferase; AST, aspartate aminotransferase; AUC, area under the curve; CI, confidence interval; CT, computed tomography; *D*, true diffusion coefficient; *D**pseudo-diffusion coefficient; DWI, diffusion-weighted imaging; *f*, pseudo-diffusion component fraction; Gd-EOB-DTPA, gadolinium ethoxybenzyl diethylenetriamine pentaacetic acid; γ-GT, γ-glutamyltransferase; HBP, hepatobiliary phase; HCC, hepatocellular carcinoma; ICC, interclass correlation coefficient; IVIM, intravoxel incoherent motion; LI-RADS, the liver imaging reporting and data system; MITK, medical imaging interaction toolkit; MRI, magnetic resonance imaging; MVI, microvascular invasion; OR, odds ratio; RFS, recurrence-free survival; APHE, arterial-phase hyperenhancement; ROC, receiver operating characteristic; ROI, region of interest; T1WI, T1-weighted image; T2WI, T2-weighted image; VETC, vessels encapsulating tumor clusters.

## Data Sharing Statement

The datasets used for analyses during the current study are available from the corresponding author on reasonable request.

## Ethics Approval and Informed Consent

This study was approved by the Institutional Review Board of Southern Medical University (2017-YXZDK-002) and was conducted following the principles of the Declaration of Helsinki. Written informed consent was obtained from all patients.

## Consent for Publication

All authors and all patients involved are agreed to the publication of this manuscript.

## Acknowledgments

The authors would like to acknowledge the support of National Science Foundation for Young Scientists of China, Natural Science Foundation of China, Guangdong Basic and Applied Basic Research Foundation and President Foundation of Zhujiang Hospital, Southern Medical University.

## Author Contributions

All authors made a significant contribution to the work reported, whether that is in the conception, study design, execution, acquisition of data, analysis and interpretation, or in all these areas; took part in drafting, revising or critically reviewing the article; gave final approval of the version to be published; have agreed on the journal to which the article has been submitted; and agree to be accountable for all aspects of the work.

## Funding

This work was funded by National Science Foundation for Young Scientists of China (82302315), Natural Science Foundation of China (82370674), Guangdong Basic and Applied Basic Research Foundation (2021A1515011305,

2023A1515012242, 2024A1515012170, 2025A1515011722) and President Foundation of Zhujiang Hospital, Southern Medical University (yzjj2021qn23).

## Disclosure

The authors report no conflicts of interest in this work.

## References


1. Mathur P, Sathishkumar K, Chaturvedi M. et al. Cancer statistics, 2020: report from national cancer registry programme, India. *JCO Glob Oncol*. 2020;6:1063–1075. doi:10.1200/go.20.00122
2. Sung H, Ferlay J, Siegel RL, et al. Global cancer statistics 2020: GLOBOCAN estimates of incidence and mortality worldwide for 36 cancers in 185 countries. *CA Cancer J Clin*. 2021;71(3):209–249. doi:10.3322/caac.21660
3. Galle PR, Forner A, Llovet JM, et al. EASL clinical practice guidelines: management of hepatocellular carcinoma. *J Hepatol*. 2018;69(1):182–236. doi:10.1016/j.jhep.2018.03.019
4. Marrero JA, Kulik LM, Sirlin CB, et al. Diagnosis, staging, and management of hepatocellular carcinoma: 2018 practice guidance by the American association for the study of liver diseases. *Hepatology*. 2018;68(2):723–750. doi:10.1002/hep.29913
5. Reig M, Forner A, Rimola J, et al. BCLC strategy for prognosis prediction and treatment recommendation: the 2022 update. *J Hepatol*. 2022;76 (3):681–693. doi:10.1016/j.jhep.2021.11.018
6. Ma X, Wei J, Gu D, et al. Preoperative radiomics nomogram for microvascular invasion prediction in hepatocellular carcinoma using contrast-enhanced CT. *Eur Radiol*. 2019;29(7):3595–3605. doi:10.1007/s00330-018-5985-y
7. Tampaki M, Papatheodoridis GV, Cholongitas E. Intrahepatic recurrence of hepatocellular carcinoma after resection: an update. *Clin J Gastroenterol*. 2021;14(3):699–713. doi:10.1007/s12328-021-01394-7
8. Fang JH, Zhou HC, Zhang C, et al. A novel vascular pattern promotes metastasis of hepatocellular carcinoma in an epithelial-mesenchymal transition-independent manner. *Hepatology*. 2015;62(2):452–465. doi:10.1002/hep.27760
9. Liu K, Dennis C, Prince DS, et al. Vessels that encapsulate tumour clusters vascular pattern in hepatocellular carcinoma. *JHEP Rep*. 2023;5 (8):100792. doi:10.1016/j.jhepr.2023.100792
10. Huang CW, Lin SE, Huang SF, et al. The vessels that encapsulate tumor clusters (VETC) pattern is a poor prognosis factor in patients with hepatocellular carcinoma: an analysis of microvessel density. *Cancers*. 2022;14(21):5428. doi:10.3390/cancers14215428
11. Chen ZY, Guo ZX, Lu LH, et al. The predictive value of vessels encapsulating tumor clusters in treatment optimization for recurrent early-stage hepatocellular carcinoma. *Cancer Med*. 2021;10(16):5466–5474. doi:10.1002/cam4.4102
12. Fang JH, Xu L, Shang LR, et al. Vessels that encapsulate tumor clusters (VETC) pattern is a predictor of sorafenib benefit in patients with hepatocellular carcinoma. *Hepatology*. 2019;70(3):824–839. doi:10.1002/hep.30366
13. Wang JH, Li XS, Tang HS, et al. Vessels that encapsulate tumor clusters (VETC) pattern predicts the efficacy of adjuvant TACE in hepatocellular carcinoma. *J Cancer Res Clin Oncol*. 2023;149(8):4163–4172. doi:10.1007/s00432-022-04323-4
14. Feng Z, Li H, Zhao H, et al. Preoperative CT for characterization of aggressive macrotrabecular-massive subtype and vessels that encapsulate tumor clusters pattern in hepatocellular carcinoma. *Radiology*. 2021;300(1):219–229. doi:10.1148/radiol.2021203614
15. Fan Y, Yu Y, Hu M, et al. Imaging features based on Gd-EOB-DTPA-enhanced MRI for predicting vessels encapsulating tumor clusters (VETC) in patients with hepatocellular carcinoma. *Br J Radiol*. 2021;94(1119):20200950. doi:10.1259/bjr.20200950
16. Yu Y, Fan Y, Wang X, et al. Gd-EOB-DTPA-enhanced MRI radiomics to predict vessels encapsulating tumor clusters (VETC) and patient prognosis in hepatocellular carcinoma. *Eur Radiol*. 2022;32(2):959–970. doi:10.1007/s00330-021-08250-9
17. Fan Y, Yu Y, Wang X, et al. Texture analysis based on Gd-EOB-DTPA-enhanced MRI for identifying vessels encapsulating tumor clusters (VETC)-positive hepatocellular carcinoma. *J Hepatocell Carcinoma*. 2021;8:349–359. doi:10.2147/jhc.S293755
18. Yang J, Dong X, Wang G, et al. Preoperative MRI features for characterization of vessels encapsulating tumor clusters and microvascular invasion in hepatocellular carcinoma. *Abdom Radiol*. 2023;48(2):554–566. doi:10.1007/s00261-022-03740-w
19. Le Bihan D, Breton E, Lallemand D, Aubin ML, Vignaud J, Laval-Jeantet M. Separation of diffusion and perfusion in intravoxel incoherent motion MR imaging. *Radiology*. 1988;168(2):497–505. doi:10.1148/radiology.168.2.3393671
20. Kang HJ, Kim H, Lee DH, et al. Gadoxetate-enhanced MRI features of proliferative hepatocellular carcinoma are prognostic after surgery. *Radiology*. 2021;300(3):572–582. doi:10.1148/radiol.2021204352
21. Mulé S, Galletto Pregliasco A, Tenenhaus A, et al. Multiphase liver MRI for identifying the macrotrabecular-massive subtype of hepatocellular carcinoma. *Radiology*. 2020;295(3):562–571. doi:10.1148/radiol.2020192230
22. Wei Y, Huang Z, Tang H, et al. IVIM improves preoperative assessment of microvascular invasion in HCC. *Eur Radiol*. 2019;29(10):5403–5414. doi:10.1007/s00330-019-06088-w
23. Chernyak V, Fowler KJ, Kamaya A, et al. Liver Imaging Reporting and Data System (LI-RADS) version 2018: imaging of hepatocellular carcinoma in at-risk patients. *Radiology*. 2018;289(3):816–830. doi:10.1148/radiol.2018181494
24. American College of Radiology. Liver imaging reporting and data system, LI- RADS lexicon. 2020.
25. Tohme S, Yazdani HO, Liu Y, et al. Hypoxia mediates mitochondrial biogenesis in hepatocellular carcinoma to promote tumor growth through HMGB1 and TLR9 interaction. *Hepatology*. 2017;66(1):182–197. doi:10.1002/hep.29184
26. Wu B, Jia F, Li X, Li L, Wang K, Han D. Comparative study of amide proton transfer imaging and intravoxel incoherent motion imaging for predicting histologic grade of hepatocellular carcinoma. *Front Oncol*. 2020;10:562049. doi:10.3389/fonc.2020.562049
27. Zhang Y, Kuang S, Shan Q, et al. Can IVIM help predict HCC recurrence after hepatectomy? *Eur Radiol*. 2019;29(11):5791–5803. doi:10.1007/s00330-019-06180-1
28. Yang C, Wei XQ, Zheng J, et al. A correlative study between IVIM-DWI parameters and VEGF and MMPs expression in hepatocellular carcinoma. *Quant Imaging Med Surg*. 2023;13(3):1887–1898. doi:10.21037/qims-22-271

29. Khatib S, Pomyen Y, Dang H, Wang XW. Understanding the cause and consequence of tumor heterogeneity. *Trends Cancer*. 2020;6(4):267–271. doi:10.1016/j.trecan.2020.01.010
30. Le Bihan D. What can we see with IVIM MRI? *Neuroimage*. 2019;187:56–67. doi:10.1016/j.neuroimage.2017.12.062
31. Colecchia A, Schiumerini R, Cucchetti A, et al. Prognostic factors for hepatocellular carcinoma recurrence. *World J Gastroenterol*. 2014;20 (20):5935–5950. doi:10.3748/wjg.v20.i20.5935
32. Jonas S, Bechstein WO, Steinmüller T, et al. Vascular invasion and histopathologic grading determine outcome after liver transplantation for hepatocellular carcinoma in cirrhosis. *Hepatology*. 2001;33(5):1080–1086. doi:10.1053/jhep.2001.23561
33. Kim SU, Jung KS, Lee S, et al. Histological subclassification of cirrhosis can predict recurrence after curative resection of hepatocellular carcinoma. *Liver Int*. 2014;34(7):1008–1017. doi:10.1111/liv.12475
34. Lauwers GY, Terris B, Balis UJ, et al. Prognostic histologic indicators of curatively resected hepatocellular carcinomas: a multi-institutional analysis of 425 patients with definition of a histologic prognostic index. *Am J Surg Pathol*. 2002;26(1):25–34. doi:10.1097/00000478-200201000-00003
35. Renzulli M, Brocchi S, Cucchetti A, et al. Can current preoperative imaging be used to detect microvascular invasion of hepatocellular carcinoma? *Radiology*. 2016;279(2):432–442. doi:10.1148/radiol.2015150998
36. Ding T, Xu J, Zhang Y, et al. Endothelium-coated tumor clusters are associated with poor prognosis and micrometastasis of hepatocellular carcinoma after resection. *Cancer*. 2011;117(21):4878–4889. doi:10.1002/cncr.26137
37. Rhee H, An C, Kim HY, Yoo JE, Park YN, Kim MJ. Hepatocellular carcinoma with irregular rim-like arterial phase hyperenhancement: more aggressive pathologic features. *Liver Cancer*. 2019;8(1):24–40. doi:10.1159/000488540
38. Li X, Qi Z, Du H, et al. Deep convolutional neural network for preoperative prediction of microvascular invasion and clinical outcomes in patients with HCCs. *Eur Radiol*. 2022;32(2):771–782. doi:10.1007/s00330-021-08198-w
39. Li X, Liang X, Li Z, et al. A novel stratification scheme combined with internal arteries in CT imaging for guiding postoperative adjuvant transarterial chemoembolization in hepatocellular carcinoma: a retrospective cohort study. *Int J Surg*. 2024;110(5):2556–2567. doi:10.1097/js9.0000000000001191
40. Ma WJ, Wang HY, Teng LS. Correlation analysis of preoperative serum alpha-fetoprotein (AFP) level and prognosis of hepatocellular carcinoma (HCC) after hepatectomy. *World J Surg Oncol*. 2013;11:212. doi:10.1186/1477-7819-11-212
41. Xia Y, Yan ZL, Xi T, et al. A case-control study of correlation between preoperative serum AFP and recurrence of hepatocellular carcinoma after curative hepatectomy. *Hepatogastroenterology*. 2012;59(119):2248–2254. doi:10.5754/hge11978